Sequence-Specific ^1H and ^{15}N Resonance Assignments for Human Dihydrofolate Reductase in Solution†

Brian J. Stockman,‡,§ N. R. Nirmala,‡ Gerhard Wagner,*,‡ Tavner J. Delcamp,∥ Michael T. DeYarman,∥ and James H. Freisheim∥

Department of Biological Chemistry and Molecular Pharmacology, Harvard Medical School, Boston, Massachusetts 02115, and Department of Biochemistry and Molecular Biology, Medical College of Ohio, Toledo, Ohio 43699

Received July 17, 1991; Revised Manuscript Received September 25, 1991

ABSTRACT: Dihydrofolate reductase is an intracellular target enzyme for folate antagonists, including the anticancer drug methotrexate. In order to design novel drugs with altered binding properties, a detailed description of protein–drug interactions in solution is desirable to understand the specificity of drug binding. As a first step in this process, heteronuclear three-dimensional NMR spectroscopy has been used to make sequential resonance assignments for more than 90% of the residues in human dihydrofolate reductase complexed with methotrexate. Uniform enrichment of the 21.5-kDa protein with ^{15}N was required to obtain the resonance assignments via heteronuclear 3D NMR spectroscopy since homonuclear 2D spectra did not provide sufficient ^1H resonance dispersion. Medium- and long-range NOE's have been used to characterize the secondary structure of the binary ligand–enzyme complex in solution.

Dihydrofolate reductase (5,6,7,8-tetrahydrofolate:$NADP^+$ oxidoreductase, EC 1.5.1.3) catalyzes the NADPH-dependent reduction of 7,8-dihydrofolate to 5,6,7,8-tetrahydrofolate. Tetrahydrofolate or its derivatives are essential cofactors in the biosynthesis of purine nucleotides, thymidylate, and several amino acids. Failure to maintain adequate levels of tetrahydrofolate reduces cellular thymidylate and purine levels, resulting in decreased nucleic acid synthesis (Freisheim & Matthews, 1984). On the basis of this metabolic consequence, DHFR[1] is a pharmacologically important intracellular target enzyme for a number of folate antogonists, including the anticancer drug methotrexate and the antibacterial agent trimethoprim. Recently, *Pneumocystis carinii* DHFR has become an important anti-folate target since pneumonia induced by this fungal pathogen is the main cause of death in patients with acquired immunodeficiency syndrome (Edman et al., 1989).

X-ray diffraction techniques have been used to elucidate the structure of a variety of DHFR's with and without bound ligands, including *Lactobacillus casei* (Bolin et al., 1982), *Escherichia coli* (Bolin et al., 1982; Bystroff et al., 1990; Bystroff & Kraut, 1991), chicken liver (Matthews et al., 1985a,b), mouse L1210 cells (Stammers et al., 1987), and human (Oefner et al., 1988; Davies et al., 1990). Likewise, solution NMR spectroscopy has been used to investigate the structure and ligand-binding interactions of DHFR isolated from *L. casei* (Birdsall et al., 1989; Carr et al., 1991), *E. coli* (Falzone et al., 1990, 1991), and human (Stockman et al., 1991). Folate substrates and inhibitors have been shown to bind in a 15-Å deep cavity across one face of the enzyme. Although the folding topology is similar among the various DHFR's, subtle changes in the active site have been found to have profound changes on binding affinity of and specificity for ligands (Blakley, 1984; Matthews et al., 1985a).

Solution NMR spectroscopy provides structural information complementary to crystallography. While a single crystal structure in one crystal form usually gives a detailed picture of the conformation of a protein, it may represent, because of the bias of crystal contacts, only a subset of the possible conformations that are present in solution. Therefore, in the field of X-ray crystallography it is considered valuable to solve structures in different crystal forms in order to obtain an impression of the accuracy of the structures or to evaluate the spread of possible conformations. An NMR structure determination in solution complements this by providing a picture of the protein in the aqueous medium. While the overall folding topology of a protein may be identical in the solution and the crystalline state, surface features may differ as determined from the two techniques (Wagner et al., 1991). Differences may be physiologically important, especially as regards protein–protein or protein–ligand interactions. Ligand-induced conformational changes can be monitored by NMR spectroscopy as a function of ligand chemical structure and of residues comprising the binding site. In addition, NMR spectroscopy can elucidate dynamic properties of proteins or enzymes and how these properties may vary upon ligand binding. Understanding the interactions between anti-folate drugs and human DHFR that are responsible for the specificity of binding and induced conformational changes may lead to the development of new anti-folate drugs with altered or improved specificity.

As a first step toward this goal, three-dimensional heteronuclear NMR spectroscopy (Zuiderweg & Fesik, 1989; Marion et al., 1989) has been used to sequentially assign the

† Supported by NIH Grant GM 38608 to G.W., NIH Grant CA 41467 to J.H.F., and Damon Runyon-Walter Winchell Cancer Research Fund Fellowship DRG-1062 to B.J.S.

‡ Harvard Medical School.

§ Present address: Physical and Analytical Chemistry, The Upjohn Company, 301 Henrietta St., Kalamazoo, MI 49007.

∥ Medical College of Ohio.

[1] Abbreviations: amino acids are denoted by the standard one-letter code; DHFR, dihydrofolate reductase; DQF-COSY, double-quantum filtered correlation spectroscopy; HMQC, heteronuclear multiple-quantum coherence; HSQC, heteronuclear single-quantum correlation; INEPT, insensitive nuclei enhancement by polarization transfer; GARP, globally optimized alternating phase rectangular pulse; NMR, nuclear magnetic resonance; NOE, nuclear Overhauser enhancement; NOESY, nuclear Overhauser enhancement spectroscopy; SCUBA, stimulated cross peaks under bleached alphas; TOCSY, total correlation spectroscopy.

0006-2960/92/0431-218$03.00/0

^1H and ^{15}N resonances of human DHFR in solution. Analysis of medium- and long-range NOE's has permitted determination of the enzyme's solution secondary structure and will provide the basis upon which to elucidate the solution tertiary structure. Key resonances from residues in the folate binding site have been assigned. NOE contacts with bound ligands will allow these resonances to serve as probes of conformation changes resulting from mutations and altered ligands, as well as to characterize the conformation of bound drugs.

Materials and Methods

Protein Enrichment and Sample Preparation. Recombinant human DHFR was prepared as previously described (Prendergast et al., 1988). Uniformly ^{15}N-enriched protein was prepared by using M9 minimal media and substituting ^{15}N-H_4Cl in place of $^{14}NH_4Cl$ as the sole nitrogen source. Protein selectively ^{15}N-enriched at the amide nitrogen positions of leucine, valine, isoleucine, and alanine residues was prepared by supplementing the M9 minimal media with [^{15}N]leucine. Since a prototrophic *E. coli* strain (JM107) was used, the ^{15}N label was scrambled to valine, isoleucine, and, to a lesser extent, alanine amide nitrogens because of transamination reactions (McIntosh & Dahlquist, 1990). Label scrambling proved beneficial during the assignment process. Samples for NMR spectroscopy typically contained 1–2 mM DHFR–methotrexate binary complex and 25 mM KCl in 50 mM phosphate buffer at pH 6.5. The binary complex (Reddy et al., 1978) was stable over the course of the NMR measurements as judged by the appearance of subsequent NMR spectra. The catalytic activity of the enzyme was not measured after data acquisition since methotrexate cannot be displaced without denaturing the enzyme. Samples dissolved in ^2H_2O were prepared by repeatedly concentrating the solution using an Amicon microultrafiltration system.

NMR Spectroscopy. All NMR spectra were recorded at 298 K on a General Electric Ω-500 (11.7 Tesla) or Bruker AMX-600 (14.2 Tesla) spectrometer. Proton chemical shifts were referenced to the ^1H_2O signal at 4.76 ppm (298 K). Nitrogen chemical shifts were referenced to external $^{15}NH_4Cl$ (2.9 M) in 1 M HCl at 24.93 ppm.

Two-dimensional NOESY (Anil Kumar et al., 1980) and DQF-COSY (Piantini et al., 1982) were recorded as described previously (Stockman et al., 1991). Two-dimensional ^1H–^{15}N HSQC spectra (Bodenhausen & Ruben, 1980) were acquired using nonrefocused and reverse INEPT magnetization transfers (Morris & Freeman, 1979) to achieve narrow line widths, thereby maximizing spectral resolution (Bax et al., 1990). The ^{15}N and ^1H sweep widths used were 4000 Hz and 11 111 Hz, respectively. Acquisition of the complete ^1H–^{15}N 2D spectrum recorded in both dimensions, without folding in resonances, provided the basis for determining the reduced sweep widths that were used to record 3D spectra. Spectral folding is necessary in 3D spectra in order to achieve sufficient resolution. A total of 350 increments were acquired, each the sum of 96 scans. Continuous wave low-power saturation was used during the 1.0-s relaxation delay to reduce the intensity of the ^1H_2O resonance. GARP decoupling (Shaka et al., 1985) was used during acquisition to decouple ^{15}N. Spectra were recorded on human DHFR in ^1H_2O and ^2H_2O as solvent to determine which $^1H^N$ resonances had retarded exchange rates.

Three-dimensional NOESY-HMQC and TOCSY-HMQC spectra were acquired with slight modification (Clubb et al., 1991) of the methods described by Zuiderweg and Fesik (1989) and Marion et al. (1989). As with the 2D HSQC spectrum, low-power continuous wave saturation was used during the 1.3-s relaxation delay to reduce the ^1H_2O resonance intensity. The SCUBA method (Brown et al., 1988) was used to recover intensity of saturated $^1H^\alpha$ resonances resulting from irradiation of the solvent line. Decoupling of ^{15}N during the t_1 period and during acquisition was accomplished using an MLEV-64 sequence (Levitt & Freeman, 1981). Sweep widths of 8604, 2000, and 10 000 Hz were used in the ω_1, ω_2, and ω_3 dimensions, respectively. Each 3D spectrum was recorded as a series of 2D ^1H–^1H data sets with varying t_2 increments.

Each 3D spectrum consisted of 256 t_1 values for each t_2 value. A total of 32 t_2 values were acquired for the TOCSY-HMQC spectrum, while 36 t_2 values were recorded for the NOESY-HMQC spectrum. For each t_1 value, 32 scans were collected, each containing 1024 complex data points. The NOESY-HMQC experiment was acquired with a mixing time of 100 ms. The TOCSY-HMQC experiment was collected with an MLEV-17 spin lock (Levitt & Freeman, 1981; Bax & Davis, 1985) time of 40 ms. Total acquisition time for each 3D experiment was 120 h.

Data were processed using the program FELIX from Hare Research, Inc. Artifacts stemming from the residual ^1H_2O resonance were removed using a dispersive baseline correction routine (Adler & Wagner, 1991) after Fourier transformation in t_3 but prior to Fourier transformation in t_1 and t_2. After elimination of the aliphatic half of the spectrum in ω_3 and zero filling in each dimension, a final frequency domain data set of 1024 × 64 × 512 real points in ω_1, ω_2, and ω_3, respectively, was obtained. In-house written software was used to facilitate hard copy plots of two-dimensional ω_1–ω_3 planes of the three-dimensional spectra on a Hewlett-Packard DraftMaster RX plotter.

Results

The high (by NMR standards) molecular mass of the DHFR–methotrexate complex (21.5 kDa) gave rise to relatively large resonance line widths compared to smaller proteins. This resulted in increased cancellation of antiphase cross peaks in DQF-COSY spectra, as well as poor magnetization transfer in TOCSY spectra. As a consequence, less than 20% of the amino acid side-chain spin systems could be delineated reliably using a combination of these two-dimensional ^1H–^1H spectra. In addition, the large number of proton resonances resulted in highly-overlapped two-dimensional NOESY spectra. Consequently, traditional sequential assignment strategies (Wüthrich, 1986) were unsuccessful.

To overcome these limitations, a heteronuclear three-dimensional NMR approach was used (Zuiderweg & Fesik, 1989; Marion et al., 1989). Uniform enrichment of DHFR with ^{15}N allowed resolution of the crowded amide proton region by spreading the resonances into the ^{15}N dimension. Figure 1 shows the two-dimensional ^1H–^{15}N HSQC spectrum of human DHFR. The almost complete lack of overlap is readily apparent. Assignments indicated will be discussed below. An identical experiment recorded on a sample containing human DHFR that was ^{15}N enriched at leucine, isoleucine, valine, and alanine N^α positions allowed the subset of correlations arising from these types of amino acids to be identified, facilitating the assignment process.

The resolution afforded by the ^{15}N frequency dimension was exploited to spread two-dimensional TOCSY and NOESY spectra into a third dimension. Analysis of the now-simplified two-dimensional ^1H–^1H planes of the three-dimensional TOCSY-HMQC and NOESY-HMQC spectra, in a manner completely analogous to conventional assignment techniques (Wüthrich, 1986), resulted in essentially complete backbone and many side-chain resonance assignments for the non-prolyl residues. Since a discussion of each assignment would be too

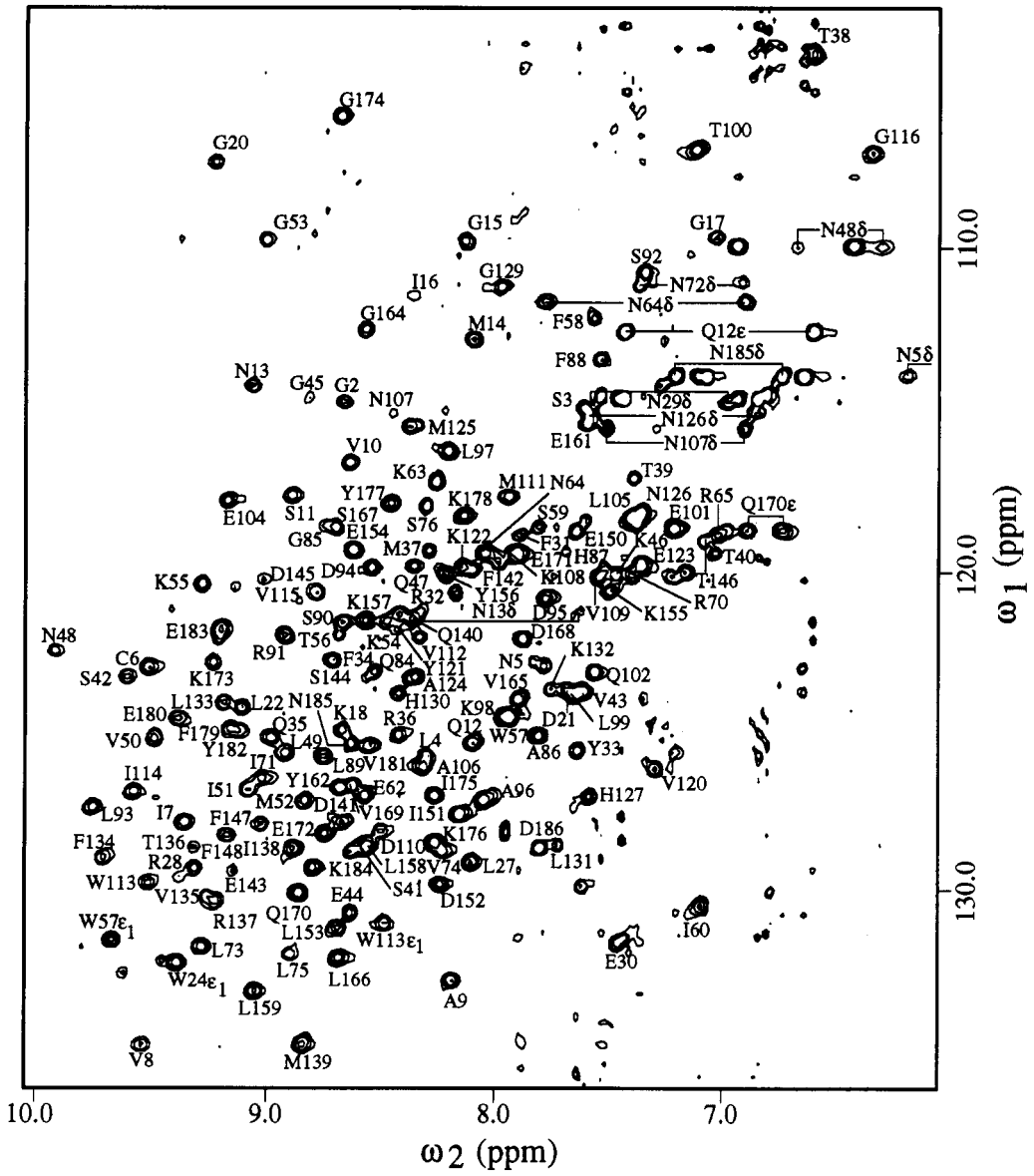

FIGURE 1: Region of the 14.2-T ^1H–^{15}N HSQC spectrum of uniformly ^{15}N-enriched human DHFR. Assigned correlations are labeled according to residue type and sequence number, and, for correlations other than amide backbone nitrogens, atom type. Correlations for the backbone amide groups of N19, W24, N29, and N72 are outside the spectral region shown.

lengthy, only a few representative stretches of assignments will be presented. To illustrate subtleties in the assignment strategy resulting from differences in backbone topology, detailed assignments of residues from α-helical and β-sheet stretches will be discussed.

The regular geometry of an α-helical stretch of residues is manifested in several ways in the 3D NOESY-HMQC and 3D TOCSY-HMQC spectra: strong d_{NN} NOE's between amide protons of adjacent residues, medium intraresidue $d_{N\alpha}$ and interresidue $d_{N\alpha}(i,i-1)$ NOE's, weak $d_{N\alpha}(i,i-3)$ NOE's, and weak $d_{N\alpha}$ scalar correlations in TOCSY spectra. Each d_{NN} NOE occurs twice in the 3D NOESY-HMQC spectrum, once in the ^{15}N plane (ω_2) containing each direct ^1H–^{15}N correlation. Provided that the $^1H^N$ chemical shifts are not degenerate, the d_{NN} pairs are easily identified. Analysis of intraresidue TOCSY correlations and interresidue NOESY correlations allows the sequential orientation of the paired residues to be determined.

An example of a stretch of residues showing these characteristics is shown in Figure 2. Each panel represents a portion of an ω_1,ω_3 slice taken at the ω_2 frequency of the indicated residue. Each slice spans 0.31 ppm (17 data points) in ω_3 and contains correlations involving the backbone amide proton of the indicated residue. In each panel, the direct ^1H–^{15}N correlation is located in the ω_1 dimension at the $^1H^N$ chemical shift listed in Table I and is centered in the ω_3 dimension. Intraresidue correlations, identified by comparison with the corresponding slice at the same ^{15}N frequency in the 3D TOCSY-HMQC spectrum, are boxed. Sequential $d_{N\alpha}(i,i-1)$ connectivities for each residue are indicated by arrows connecting the intraresidue $d_{N\alpha}$ correlation in one panel to the interresidue $d_{N\alpha}(i,i-1)$ correlation in the adjacent panel. Arrows also identify sequential $d_{N\beta}(i,i-1)$ correlations observed for D95, A96, and L99. Redundant d_{NN} connectivities, observed for each pair of adjacent residues, are indicated by horizontal lines. The d_{NN} correlations are especially useful to make sequential assignments when the $^1H^\alpha$ resonances of adjacent residues are nearly degenerate, such as is the case for D94–D95 in Figure 2. Other connectivities, such as the $d_{N\alpha}(i,i-2)$ and $d_{N\beta}(i,i-1)$ NOE's, verify the D95 assignment.

Placement of this stretch of connectivities in the primary sequence was accomplished using two criteria: (1) the fourth residue was assigned as an alanine on the basis of scalar correlation spectra, and (2) three of these residues (1, 5, and

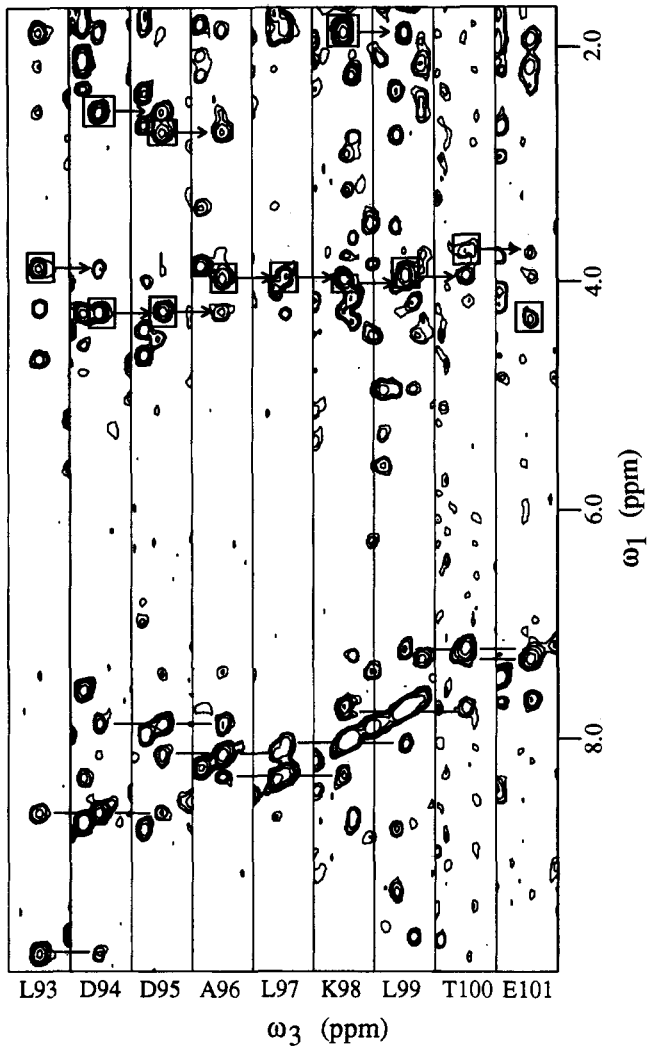

FIGURE 2: Selected ω_1,ω_3 slices taken from the 11.7-T $^1H-^{15}N$ HMQC-NOESY spectrum of human DHFR. Slices are taken at the ω_2 frequency corresponding to the $^{15}N^{\alpha}$ atom of the indicated residues. Each slice represents 0.31 ppm in ω_3, with the center located at the frequency of the indicated $^1H^N$ resonance (listed in Table I). Intraresidue $d_{N\alpha}$ correlations are boxed. Sequential d_{NN} correlations are identified by horizontal lines between adjacent panels. Sequential interresidue $d_{N\alpha}(i,i-1)$ and $d_{N\beta}(i,i-1)$ correlations are indicated by arrows beginning at the boxed intraresidue correlation in the preceding slice.

7) gave strong $^1H-^{15}N$ correlations in the 2D HSQC spectrum of the ([^{15}N]leucine)DHFR sample (the alanine also gave a correlation, although of less intensity). Only the sequence L93-D94-D95-A96-L97-K98-L99-T100-E101 satisfies these criteria (even considering scrambling of the leucine label to valine and isoleucine). Observation of strong d_{NN} NOE's, medium $d_{N\alpha}(i,i-1)$ NOE's, and, in cases of favorable resolution, $d_{N\alpha}(i,i-3)$ NOE's indicates that this stretch of residues adopts an α-helical conformation in solution. This α-helix extends one additional residue on the carboxy-terminal end (not shown) and thus comprises residues 93–102.

Roughly 35 additional pairs of d_{NN} NOE's were identified in the 3D NOESY-HMQC spectrum. Identification of sequential NOE's aligned most of these residues into four stretches, corresponding to residues 28–39, 54–60, 104–109, and 120–127. Essentially one-quarter of the sequential assignments were facilitated in this manner.

In contrast to α-helical regions, extended chain and β-sheet sequences have a much larger separation of adjacent amide protons and thus weak or absent d_{NN} NOE's. Instead, residues with this topology tend to be manifested by intense intraresidue

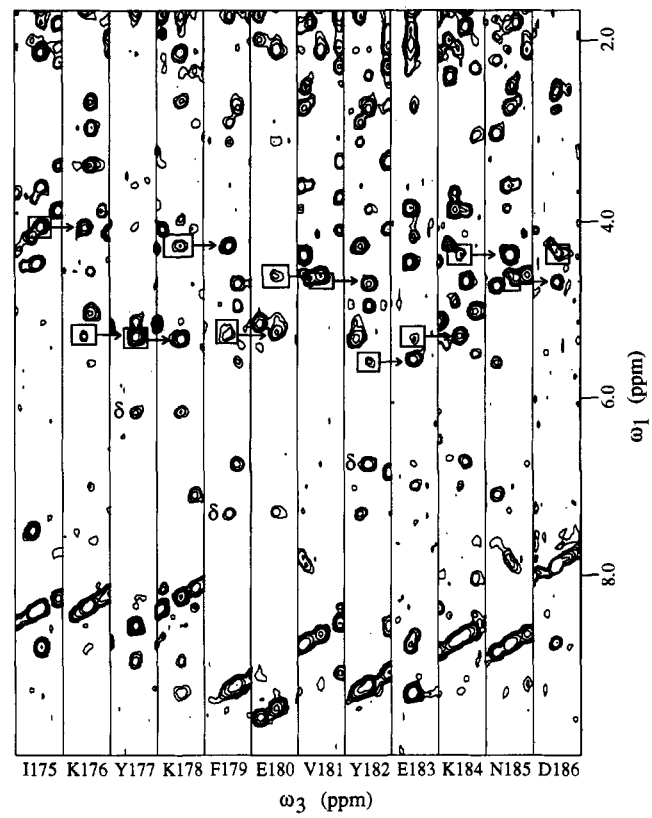

FIGURE 3: Selected ω_1,ω_3 slices taken from the 11.7-T $^1H-^{15}N$ HMQC-NOESY spectrum of human DHFR. Slices are taken at the ω_2 frequency corresponding to the $^{15}N^{\alpha}$ atom of the indicated residues. Each slice represents 0.31 ppm in ω_3, with the center located at the frequency of the indicated $^1H^N$ resonance (listed in Table I). Intraresidue $d_{N\alpha}$ correlations are boxed. Sequential $d_{N\alpha}(i,i-1)$ correlations are indicated by single-arrowhead lines beginning at the $d_{N\alpha}$ correlation in the preceding slice. Intraresidue $^1H^N-^1H^{\delta}$ NOE's for Y177, F179, and Y182 are indicated with a "δ" in the corresponding slices.

$d_{N\alpha}$ TOCSY correlations, weak or missing intraresidue $d_{N\alpha}$ NOE's, and intense interresidue $d_{N\alpha}(i,i-1)$ NOE's. In addition, the $^1H^{\alpha}$, $^1H^N$, and ^{15}N chemical shifts tend to be downfield relative to those of random coil or α-helical residues. The relative low-field chemical shifts of these atoms place the resonances in well-resolved regions in each of the three dimensions, facilitating their assignment. An example of one strand of a β-sheet is shown in Figure 3. The panels have the same format as those in Figure 2. Note the much greater intensity of the sequential $d_{N\alpha}(i,i-1)$ NOE's compared to those in Figure 2, as well as the much weaker $d_{N\alpha}$ NOE's. Also note the lack or the low intensity of d_{NN} NOE's.

Positioning of this stretch of connectivities in the primary sequence was based on several criteria: (1) two residues (1 and 7) gave strong correlations in the 2D HSQC spectrum of ([^{15}N]leucine)DHFR (thus they must be I, V, or L), (2) none of the residues are glycines, (3) three residues (3, 5, and 8) are aromatic amino acids (see below), and (4) several residues had slowly exchanging amide protons, as well as NOE's to adjacent strands of the β-sheet as predicted by the X-ray crystal structure. Only the sequence I175-K176-Y177-K178-F179-E180-V181-Y182-E183-K184-N185-D186 satisfies these requirements. The first two criteria are sufficient, since no other region of the primary sequence has two I, V, or L residues separated by five non-glycine residues. The fourth criterion is useful in that comparisons to the X-ray crystal structure often substantiate NMR data quite well. This is especially true for the backbone β-sheet core of the protein as discussed below.

Table I: Chemical Shifts of Assigned ^{1}H and ^{15}N Resonances in Human DHFR Chemical Shift (ppm)[a]

residue	N^{α}	H^{N}	H^{α}	H^{β}	others
Val 1			4.24	2.09	H^{γ} 0.90
Gly 2	114.8	8.76	3.98		
Ser 3	115.1	7.69	3.73	4.46	
Leu 4	125.7	8.36	4.51	1.43, 1.61	
Asn 5	122.8	7.89	5.62	1.23	H^{δ} 5.23, 6.29; N^{δ} 114.1
Cys 6	123.0	9.59	5.64	2.99	
Ile 7	127.8	9.43	6.26	1.29	
Val 8	134.6	9.62	4.65	2.12	H^{γ} 0.53, 0.58
Ala 9	132.7	8.28	5.18	1.13	
Val 10	116.8	8.72	5.39	1.97	H^{γ} 0.57, 0.79
Ser 11	117.8	8.98	5.13	4.45, 5.42	
Gln 12	125.4	8.18	4.18		H^{ϵ} 6.69, 7.52; N^{ϵ} 112.6
Asn 13	114.3	9.15	4.83	2.85, 3.29	H^{δ} 7.71, 8.51; N^{δ} 121.3
Met 14	112.9	8.18	4.44	2.84	
Gly 15	109.9	8.22	3.94, 4.24		
Ile 16	111.5	8.44	4.89		
Gly 17	109.8	7.12	3.63, 4.38		
Lys 18	125.0	8.76	4.28		
Asn 19	133.6	10.61	4.25	2.52, 2.89	
Gly 20	107.5	9.31	3.53, 4.07		
Asp 21	123.7	7.77	4.95	2.39, 2.76	
Leu 22	124.2	9.19	3.89	−0.22, 1.27	H^{γ} 1.50; H^{δ} 0.51, 0.80
Pro 23					
Trp 24	109.2	5.21		2.36, 2.52	$H^{\delta 1}$ 7.24; $H^{\epsilon 2}$ 6.91; $H^{\eta 2}$ 7.15, $H^{\epsilon 3}$ 6.63; $H^{\zeta 3}$ 6.95, $H^{\epsilon 1}$ 9.47; $N^{\epsilon 1}$ 132.2
Pro 25					
Pro 26					
Leu 27	129.1	8.18	4.43	1.58	
Arg 28	129.2	9.39	3.97		
Asn 29	122.1	11.10	4.68	2.82, 3.14	H^{δ} 7.07, 7.64; N^{δ} 114.8
Glu 30	131.5	7.54	4.12		
Phe 31	118.9	7.96	4.10	2.97, 3.07	H^{δ} 6.77; H^{ϵ} 6.54; H^{ζ} 7.08
Arg 32	120.7	8.26	4.11		
Tyr 33	125.6	7.73	4.12	3.09, 3.32	H^{δ} 6.75
Phe 34	123.2	8.61	4.10		
Gln 35	125.2	9.07	4.11		
Arg 36	125.1	8.51	3.75		
Met 37	119.4	8.37	3.84		
Thr 38	104.0	6.70	1.94	3.08	H^{γ} −0.21
Thr 39	117.1	7.48	3.95		
Thr 40	119.4	7.12	3.96	4.17	H^{γ} 1.13
Ser 41	128.7	8.71	4.92	3.71, 3.96	
Ser 42	123.3	9.69	4.46		
Val 43	123.8	7.69	4.19	1.63	H^{γ} 0.83, 0.85
Glu 44	130.6	8.71	4.07	1.93, 2.25	
Gly 45	114.7	8.89	3.69, 4.23		
Lys 46	120.2	7.56	4.73		
Gln 47	120.0	8.45	4.83	1.81	
Asn 48	122.5	9.98	5.49	2.81, 3.22	H^{δ} 6.40, 6.77; N^{δ} 110.1
Leu 49	125.6	9.00	5.16		
Val 50	125.2	9.57	5.42		
Ile 51	126.8	9.16	5.05	1.69	
Met 52	127.2	8.92	5.68		
Gly 53	109.8	9.08			
Lys 54	121.6	8.56	3.82		
Lys 55	120.5	9.33	4.24	2.23	
Thr 56	122.0	8.77	3.80	4.38	
Trp 57	124.5	8.01	3.39	2.93, 3.24	$H^{\delta 1}$ 4.68; $H^{\epsilon 2}$ 7.39; $H^{\eta 2}$ 6.27; $H^{\epsilon 3}$ 7.86; $H^{\zeta 3}$ 7.27; $H^{\epsilon 1}$ 9.74; $N^{\epsilon 1}$ 131.4
Phe 58	112.3	7.65	4.08	2.81	H^{δ} 7.53; H^{ϵ} 7.41; H^{ζ} 7.57
Ser 59	118.7	7.90	4.42	4.07	
Ile 60	130.4	7.19	3.65	1.06	$H^{\gamma 2}$ 0.22
Pro 61					
Glu 62	126.9	8.65	3.38		
Lys 63	117.3	8.34	4.09	1.70	
Asn 64	119.4	8.13	4.72	2.35, 2.92	H^{δ} 6.99, 7.86; N^{δ} 111.7
Arg 65	118.9	7.10	4.01	1.18	H^{ϵ} 6.37; N^{ϵ} 87.1
Pro 66					
Leu 67					
Lys 68					
Gly 69					
Arg 70	120.2	7.49	4.70		H^{ϵ} 5.87; N^{ϵ} 87.1
Ile 71	126.4	9.10	4.24	1.71	$H^{\gamma 2}$ 0.99
Asn 72	133.5	12.89	5.15		H^{δ} 7.00; 7.45; N^{δ} 111.1
Leu 73	131.7	9.36	5.03		
Val 74	128.7	8.31	4.90	1.29	$H^{\gamma 2}$ 0.09, 0.47
Leu 75	131.8	8.98	5.15		
Ser 76	118.0	8.39	4.68		
Arg 77					

Table I (Continued)

residue	N^{α}	H^{N}	H^{α}	H^{β}	others
Glu 78					
Leu 79					
Lys 80					
Glu 81					
Pro 82					
Pro 83					
Gln 84	123.3	8.50	3.89		
Gly 85	118.7	8.82	3.44, 4.46		
Ala 86	125.1	7.89	3.53	0.16	
His 87	120.0	7.61	4.06	2.78, 3.20	$H^{\delta 2}$ 7.05; $H^{\epsilon 1}$ 8.13
Phe 88	113.5	7.62	4.73	2.21	H^{δ} 7.06; H^{ϵ} 7.25
Leu 89	125.7	8.83	5.60	1.57	
Ser 90	121.6	8.75	4.89	3.41, 3.80	
Arg 91	122.0	9.01	4.33	1.87	
Ser 92	110.8	7.44	4.69	3.96, 4.27	
Leu 93	127.3	9.83	3.89		
Asp 94	120.0	8.62	4.30	2.57	
Asp 95	120.9	7.87	4.26	2.74	
Ala 96	127.2	8.13	4.01	1.37	
Leu 97	116.4	8.29	3.96		
Lys 98	124.5	8.03	4.01	1.89	
Leu 99	123.8	7.73	3.93		H^{γ} 1.41; H^{δ} 0.43, 0.60
Thr 100	107.0	7.21	3.77	4.19	H^{γ} 1.15
Glu 101	118.8	7.30	4.34	1.95	
Gln 102	123.2	7.65	4.49	2.11	
Pro 103					
Glu 104	117.9	9.26	4.08	2.00	
Leu 105	118.4	7.50	4.52	1.37, 1.54	
Ala 106	126.1	8.40	4.19	1.23	
Asn 107	115.2	8.53	4.65	2.84	H^{δ} 6.99, 7.60; N^{δ} 115.6
Lys 108	119.6	7.95	4.55		
Val 109	120.2	7.62	5.03	1.99	H^{γ} 0.84, 0.91
Asp 110	128.1	8.58	4.99	3.04	
Met 111	117.8	8.02	4.34	1.67, 2.17	
Val 112	122.1	8.41	4.81	1.99	H^{γ} 0.86
Trp 113	129.6	9.59	5.20	2.77, 2.98	$H^{\delta 1}$ 6.72; $H^{\zeta 2}$ 6.95; $H^{\eta 2}$ 5.17; $H^{\epsilon 3}$ 6.84; $H^{\zeta 3}$ 6.27; $H^{\epsilon 1}$ 8.56; $N^{\epsilon 1}$ 130.9
Ile 114	126.8	9.66	4.84	2.45	$H^{\gamma 2}$ 0.97
Val 115	120.7	8.87	5.39	2.92	
Gly 116	107.1	6.45	2.57, 4.61		
Gly 117					
Ser 118					
Ser 119					
Val 120	126.1	7.37	3.85	1.86	$H^{\gamma 2}$ 0.81, 0.94
Tyr 121	121.7	8.48	4.45	2.95, 3.13	H^{δ} 7.11; H^{ϵ} 7.03
Lys 122	120.0	8.23	3.83		
Glu 123	119.8	7.46	4.07	2.15	
Ala 124	123.3	8.42	3.83	1.46	
Met 125	115.6	8.48	4.15		
Asn 126	118.3	7.45	4.85	2.69, 2.95	H^{δ} 6.96, 7.67; N^{δ} 115.2
His 127	127.0	7.67	4.69	3.03	
Pro 128					
Gly 129	111.2	8.18	3.90, 4.15		
His 130	123.8	8.52	4.86	3.17	$H^{\delta 2}$ 7.34
Leu 131	128.4	7.80	4.94		
Lys 132	123.7	7.84	5.34	2.11	
Leu 133	124.1	9.28	5.13		
Phe 134	128.8	9.78	4.99	3.36	H^{δ} 7.34; H^{ϵ} 7.01
Val 135	130.2	9.35	4.69	2.11	H^{γ} 0.55, 0.60
Thr 136	128.6	9.40	5.11	4.02	H^{γ} 0.79
Arg 137	130.2	9.31	4.28		H^{ϵ} 8.03; N^{ϵ} 87.8
Ile 138	128.6	8.98	3.98	0.00	$H^{\gamma 2}$ −0.97
Met 139	134.6	8.93	4.20		
Gln 140	121.5	8.44	4.27	1.73, 1.98	
Asp 141	127.8	8.75	4.81	2.40	
Phe 142	119.7	8.07	4.75	2.53, 3.09	H^{δ} 7.36; H^{ϵ} 7.28
Glu 143	129.3	9.23	4.28	2.01	
Ser 144	122.8	8.79	4.84		
Asp 145	120.3	9.09	4.91		
Thr 146	119.2	7.18	4.61		H^{γ} 1.27
Phe 147	127.8	9.09	5.42	2.63, 3.12	H^{δ} 7.18
Phe 148	128.2	9.26	4.77	2.79, 2.91	H^{δ} 6.97; H^{ϵ} 6.22; H^{ζ} 6.72
Pro 149					
Glu 150	118.8	7.72	3.89	1.82	
Ile 151	127.5	8.23	3.40	1.29	$H^{\gamma 2}$ −0.07
Asp 152	129.7	8.33	4.58	2.69, 2.97	
Leu 153	131.0	8.77	4.80		
Glu 154	119.4	8.70	4.30	2.12, 2.36	

Table I (Continued)

residue	N^{α}	H^{N}	H^{α}	H^{β}	others
Lys 155	120.7	7.58	4.27	1.62	
Tyr 156	120.2	8.31	4.60	2.63	H^{δ} 6.97; H^{ϵ} 6.68
Lys 157	121.6	8.63	4.69	1.45, 1.83	
Leu 158	128.7	8.65	3.90		
Leu 159	132.9	9.13	4.73		
Pro 160					
Glu 161	115.5	7.69	4.39	1.88, 2.07	
Tyr 162	126.8	8.76	4.61	2.75	H^{δ} 7.24; H^{ϵ} 6.91
Pro 163					
Gly 164	112.6	8.65	3.65, 4.17		
Val 165	123.9	7.98	4.37	2.25	H^{γ} 0.95, 1.23
Leu 166	131.9	8.76	4.44	1.84	
Ser 167	118.7	8.78	4.72	4.05	
Asp 168	122.1	7.96	4.66	2.41, 2.67	
Val 169	126.6	8.70	3.61	1.81	H^{γ} 0.81, 0.93
Gln 170	130.0	8.94	4.09		H^{ϵ} 6.83, 6.98; N^{ϵ} 118.8
Glu 171	119.6	7.99	5.14	1.74	
Glu 172	128.2	8.83	4.48	2.15	
Lys 173	122.9	9.30	3.87	1.90	
Gly 174	106.0	8.75	3.63, 4.07		
Ile 175	126.9	8.35	4.07	2.14	$H^{\gamma 2}$ 0.78
Lys 176	128.4	8.36	5.30	1.61	
Tyr 177	117.9	8.54	5.33	2.14, 2.67	H^{δ} 6.16; H^{ϵ} 6.46
Lys 178	118.3	8.22	4.30		
Phe 179	124.8	9.25	5.28	2.91, 3.12	H^{δ} 7.28
Glu 180	124.6	9.46	4.63		
Val 181	125.4	8.63	4.71	1.48	H^{γ} −0.37, 0.48
Tyr 182	125.0	9.19	5.58	2.75	H^{δ} 6.73; H^{ϵ} 6.67
Glu 183	122.1	9.30	5.30	2.09	
Lys 184	128.6	8.69	4.41		
Asn 185	125.4	8.74	4.71	2.51, 2.75	H^{δ} 6.82, 7.31; N^{δ} 114.1
Asp 186	128.6	7.87	4.33	2.56	

[a] Proton chemical shifts are ±0.01 ppm. Nitrogen chemical shifts are ±0.1 ppm.

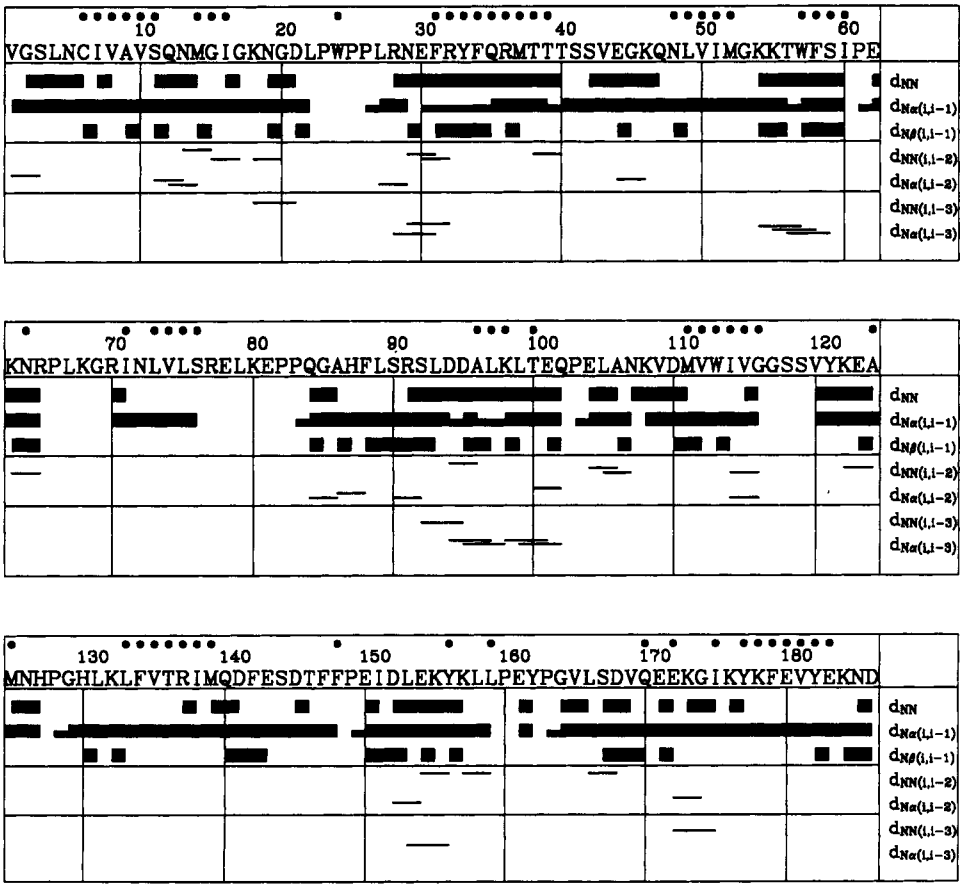

FIGURE 4: Summary of sequential assignments of human DHFR. A bar between two residues indicates assignment of a NOESY correlation between the atoms indicated on the right. Wide bars for $d_{N\alpha}(i,i-1)$ correlations indicate unambiguous NOE's, whereas narrow bars indicate NOE's that are present but, because of possible degeneracies, are not unambiguous. Several sequential proline correlations also are indicated with narrow bars, since the proline $^{1}H^{\alpha}$'s are not assigned unambiguously. Not shown are numerous $d_{N\alpha}(i,i-3)$ correlations that, because of possible degeneracies, are not assigned unambiguously. Filled circles indicate residues with slowly exchanging amide protons.

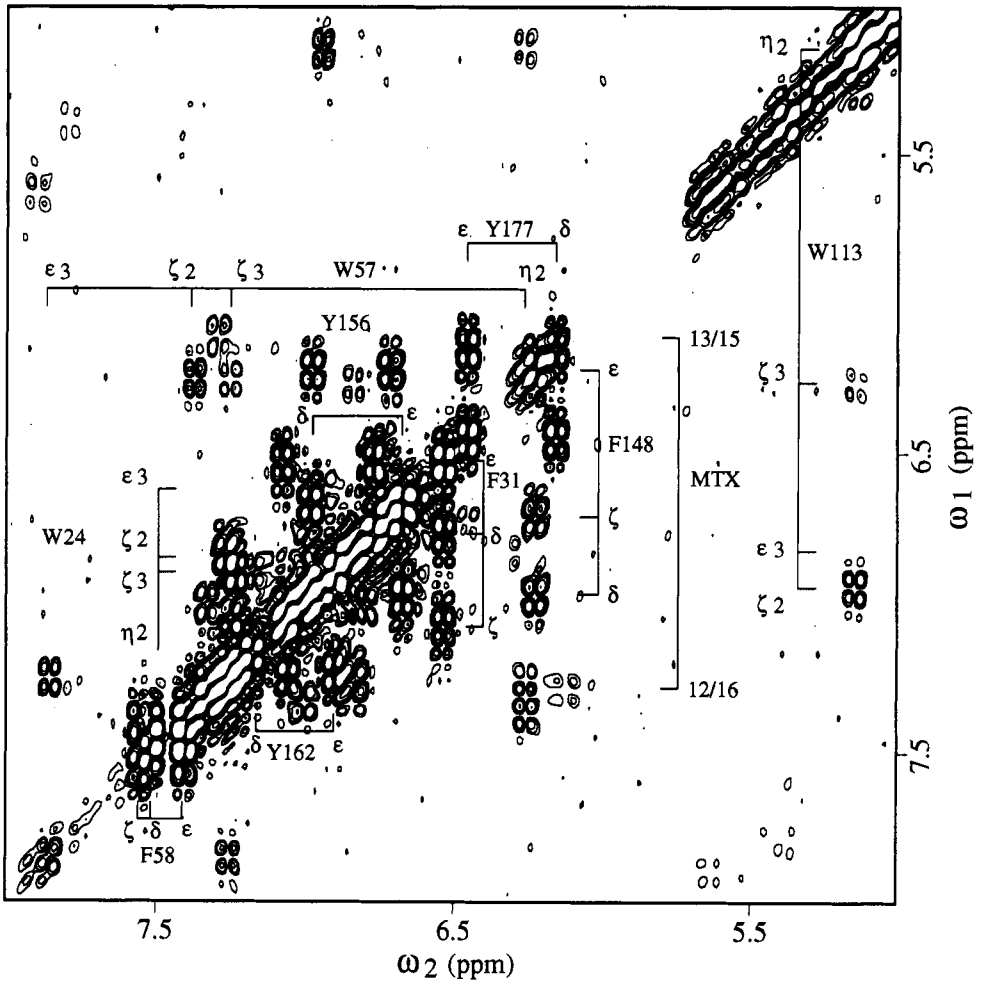

FIGURE 5: Aromatic region of the 11.7-T DQF-COSY spectrum of human DHFR. Only residues for which complete spin systems have been assigned are illustrated (see Table I). Aromatic proton resonance assignments of a given residue are identified by bars. Labeled hash marks indicate the location of each resonance. The benzene ring system protons of methotrexate (MTX) are also indicated.

Similar criteria were used to assign resonances from residues that comprise the other seven strands of the β-sheet core of human DHFR. These stretches are residues 4–11, 47–52, 71–76, 88–91, 110–116, 131–139, 157–159, and 168–171. The importance of the ([^{15}N]leucine)DHFR sample in the assignment process results from the fact that more than 40% of the β-sheet residues are leucine, valine, or isoleucine. This provided numerous reference points during the β-sheet assignment process.

The remaining residues were assigned in a manner essentially analogous to β-sheet residues. Occasionally, a strong d_{NN} NOE was observed between two or three residues not involved in the α-helices, suggesting the presence of a turn conformation in solution (Wüthrich, 1986). For instance, $^1H^N$ of G174 shows intense NOE's to the amide protons of K173 and I175. The conformation of residues 172–175 is thus a type I or I′ turn which connects two strands of the β-sheet. Further classification to one of the two classes of type I turns is not possible with NOE data alone (Wagner, 1990). Likewise residues 11–14, 18–21, and 61–64 have d_{NN} NOE's characteristic of type I or I′ turn conformations in solution, while residues 83–86 and 162–165 have d_{NN} NOE's characteristic of type II or II′ turn conformations in solution. Figure 4 summarizes the sequential and medium-range NOE's observed in human DHFR.

Analysis of a ^{1}H–^{15}N HSQC spectrum (not shown) recorded on human DHFR dissolved in ^2H_2O for 1 day revealed that close to 70 amide protons were in slow exchange with solvent. Corresponding residues are indicated in Figure 4. More than 90% of these belong to residues identified as participating in α-helices or β-strands, suggesting that their retarded exchange rates result from hydrogen-bonding characteristic of regular secondary structure. Several side-chain amide and amine protons were also observed to be in slow exchange: N48 $^1H^{\delta}$'s, R65 $^1H^{\epsilon}$, N72 $^1H^{\delta}$'s, and W113 $^1H^{\epsilon 1}$. Most likely, intramolecular hydrogen bonding accounts for these retarded exchange rates.

In some instances, assignments could be extended beyond the $^1H^{\alpha}$ position to the $^1H^{\beta}$ protons by analysis of the 3D TOCSY-HMQC spectrum. However, less than half of the residues showed TOCSY transfer to this extent, and only a few showed any TOCSY correlations beyond the $^1H^{\beta}$ position. For some side chains, especially those of methyl-containing amino acids, assignments could be made by reference to the 2D DQF-COSY spectrum (not shown). Further experiments using ^{13}C-labeled protein will be required for complete side-chain assignments (Fesik et al., 1989; Kay et al., 1990a).

The aromatic protons of many tyrosine, phenylalanine, and tryptophan side chains were assigned by observing NOE's from the main-chain amide proton to side-chain $^1H^{\beta}$ and $^1H^{\delta}$ protons. Examples of H^N–H^{δ} correlations are seen in Figure 3 at 6.14, 7.28, and 6.73 ppm for Y177, F179, and Y182, respectively. Observation of NOE's from the $^1H^{\delta}$ to the assigned $^1H^{\beta}$'s in the 2D NOESY spectrum confirmed the assignments. Extension from $^1H^{\delta}$ to the rest of the ring protons was accomplished with DQF-COSY data, as shown in Figure 5. The $^1H^{\epsilon 1}$ protons of the three tryptophan residues were easily identified in the 3D NOESY-HMQC spectrum (see Figure

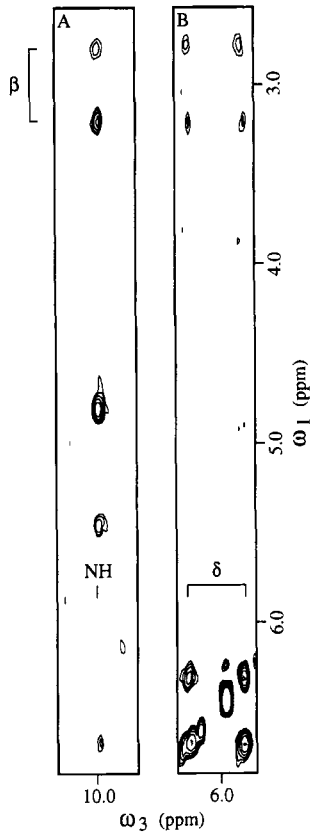

FIGURE 6: Selected ω_3,ω_1 slices from the 11.7-T ^1H–^{15}N HMQC-NOESY spectrum illustrating the assignment of the side-chain $^1H^\delta$ protons of N48. NOE's from $^1H^N$ (panel A) and both $^1H^\delta$'s (panel B) are observed to the $^1H^\beta$ protons. A weak NOE is seen in panel A between $^1H^N$ and one of the $^1H^\delta$ protons.

1). This allowed assignments to be extended to the remainder of the tryptophan side-chain protons by observation of an NOE to $^1H^{\zeta 2}$ followed by analysis of the DQF-COSY spectrum (Figure 5). Tryptophan $^1H^\delta$ resonances were assigned from $^1H^{\epsilon 1}$–$^1H^\delta$ correlations in the 3D ^1H–^{15}N TOCSY-HMQC spectrum. Several histidine side-chain protons could be assigned on the basis of sharp aromatic resonances with NOE's to previously assigned $^1H^\beta$ histidine resonances. Complete aromatic spin systems have been delineated for all three tryptophan residues, five of the six tyrosine residues, three of the nine phenylalanine residues, and one of the three histidine residues.

Nine of ten pairs of asparagine side chain $^1H^\delta$ and three of eight pairs of glutamine side-chain $^1H^\epsilon$ resonances were assigned using a similar strategy as for the aromatic side chains. Pairs of terminal $^1H^\delta$ or $^1H^\epsilon$ resonances are readily identified in the 3D NOESY-HMQC spectrum since they occur at the same ^{15}N frequency and have an intense NOE between them. NOE's from the terminal $^1H^\delta$ or $^1H^\epsilon$ protons to $^1H^\beta$ (asparagine) or $^1H\gamma$ (glutamine) were aligned with NOE's to the same protons from the $^1H^N$ resonance. An example is shown in Figure 6, which illustrates NOE's from $^1H^N$ (Figure 6A) and both $^1H^\delta$'s (Figure 6B) to both $^1H^\beta$'s of N48.

In total, we have assigned the $^1H^N$ and $^1H^\alpha$ resonances of 163 of the 174 non-prolyl residues in DHFR. Assignments have been extended to at least one $^1H^\beta$ resonance for 125 of these residues. Further side-chain assignments have been made for nearly 50% of the residues. Not including the 12 proline residues, the remaining unassigned residues are clustered in three groups: 67–69, 77–81, and 117–119. There remain six or seven unassigned correlations in the ^1H–^{15}N HSQC spectrum. Several correlations have been assigned tentatively, but conclusive assignments will require doubly $^{13}C/^{15}N$-labeled DHFR and triple-resonance strategies (Ikura et al., 1990b). Remaining ^1H–^{15}N correlations may be absent because of saturation transfer during the experiment's preparation period. In particular, this may be occurring in the 77–81 stretch, which lies on the surface of the protein and has the largest crystallographic *B* factors (Davies et al., 1990). Assignments are summarized in Table I.

Discussion

The molecular mass of hDHFR (21.5 kDa) is near the upper limit for which structures can be determined currently employing NMR spectroscopy. We have achieved nearly complete backbone assignments of this protein and characterized the secondary structure in solution. An ^{15}N-directed assignment strategy was used. The use of a valine, leucine, and isoleucine ^{15}N-enriched sample was very valuable for providing unambiguous assignments to residue types. Previously, the crystal structures of the binary human DHFR–methotrexate complex (Oefner et al., 1988) and of the binary human DHFR–folate complex (Davies et al., 1990) have been determined. Interproton distances calculated from the binary enzyme–folate complex (atomic coordinates of the enzyme–methotrexate complex are not available) were used occasionally during the assignment process to suggest possible interpretations of the NMR data.

Analysis of characteristic sequential and medium-range NOE's, combined with knowledge of $^1H^N$ exchange properties, qualitatively defines the locations of α-helices and turns. These data, in combination with key long-range NOE's, define the β-sheet framework and global fold of human DHFR in solution. Short- and medium-range NOE's are summarized in Figure 4.

α-Helices are manifested as a series of residues with d_{NN} NOE's, slowly exchanging $^1H^N$ protons, and, when resolvable, weak $d_{N\alpha}(i,i-3)$ NOE's. The criterion used to define the N-terminal boundary of the α-helices was the lack of a d_{NN} NOE to the preceding residue. C-terminal boundaries were defined as lack of a d_{NN} NOE to the subsequent residue. Often the C-terminal end of an α-helix as defined by the d_{NN} NOE criterion coincided with the end of a stretch of slowly exchanging $^1H^N$'s, providing further evidence that the characteristic hydrogen-bonding pattern of the α-helix no longer was present. However, since the shortest $^1H^N$ exchange time we have measured is on the order of 1 day, and since $^1H^N$'s at the ends of α-helices may exchange more rapidly than those in the interior, the d_{NN} NOE was used to define the C-terminal boundary. With this criterion, α-helices are located at positions [nomenclature of Davies et al. (1990)] 28–39 (αB), 54–60 (αC), 93–102 (αE), 104–109 (αE′), and 120–127 (αF).

These boundaries differ slightly from those determined by X-ray crystallography (Davies et al., 1990). The N-terminal boundaries of the αE′ helix extends through P103 and E102 in the X-ray crystal structure; lack of $^1H^N$ at P103 prohibits making this distinction with our NMR data. In addition, the N-terminus of αF extends to G117 in the X-ray crystal structure, but since residues 117–119 have yet to be assigned, the solution boundary cannot be defined. Helices αB, αE, αE′, αF, and the C-terminal half of αC are manifested by intense d_{NN} NOE's. By contrast, d_{NN} NOE's for residues 54–56 of αC are less intense by a factor of 2, suggesting that this part of the αC helix is either less ordered or more flexible than the other helices. The C-terminal boundaries of αB and αC are well defined by both d_{NN} NOE's and slow $^1H^N$ exchange. By contrast, the C-terminal boundaries of αE and αF are defined by d_{NN} NOE's but not slow $^1H^N$ exchange, suggesting that

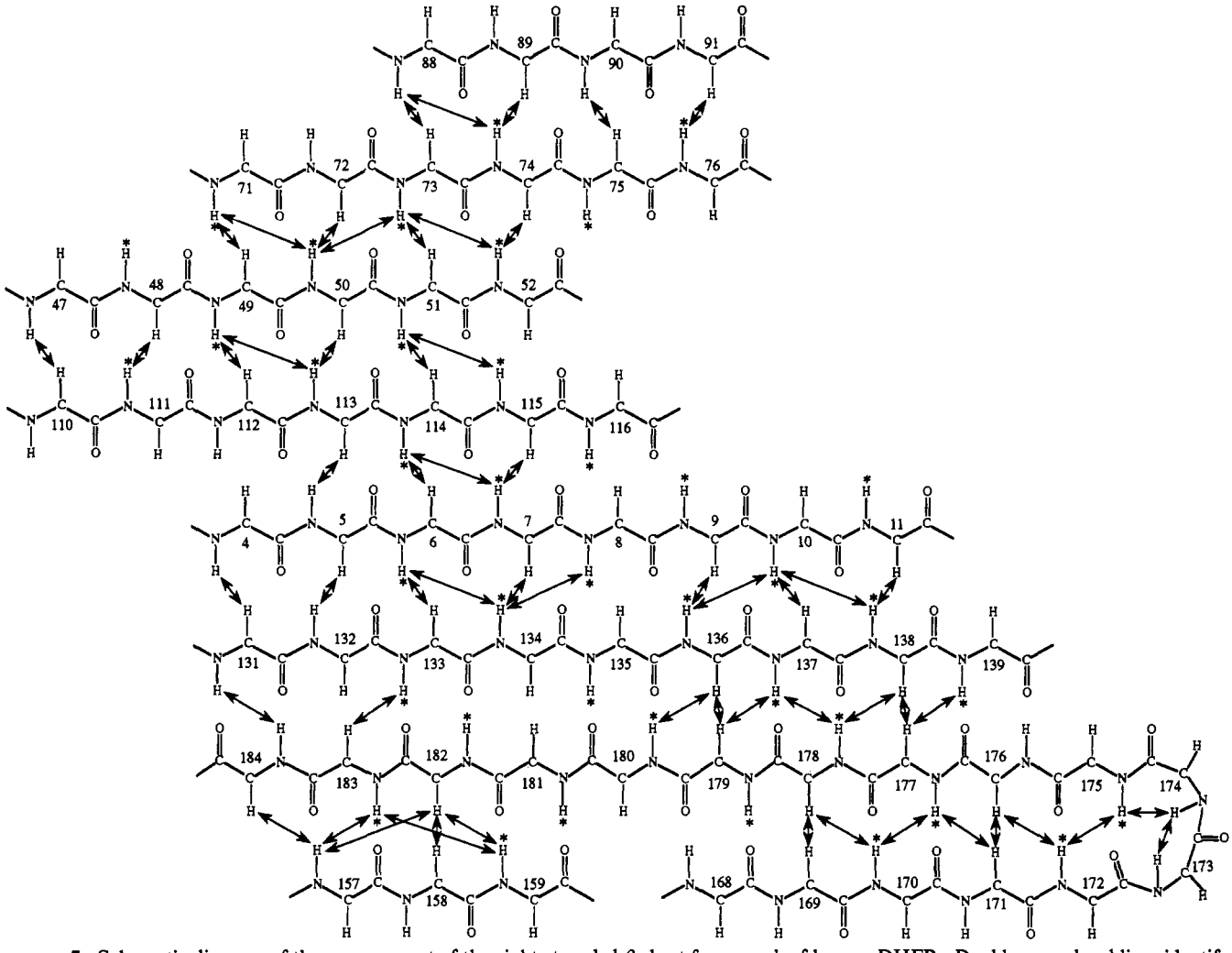

FIGURE 7: Schematic diagram of the arrangement of the eight-stranded β-sheet framework of human DHFR. Double-arrowhead lines identify assigned interstrand NOE's. Amide protons with retarded exchange rates, presumably resulting from participation in interstrand hydrogen bonds, are indicated with an asterisk.

the ends of these two helices are more flexible in solution than the others.

The X-ray crystal structure (Davies et al., 1990) of human DHFR also revealed the existence of a polyproline-like helix encompassing residues 21–26. Since our assignment strategy requires $^1H^N$ protons, only D21, L22, and W24 resonances have been assigned in this stretch. The $^1H^N$ of W24 is in slow exchange with solvent, with the next nearest slowly exchanging $^1H^N$ seven residues distant. The isolated slowly exchanging W24 $^1H^N$ may result from the spatial topology of the polyproline helix, providing evidence for the existence in solution of this localized secondary structure element.

Strands comprising β-sheet structures are manifested by stretches of residues with intense $d_{N\alpha}(i,i-1)$ NOE's and slowly exchanging $^1H^N$ protons (Figure 4). Identification of numerous interstrand NOE's from the 3D NOESY-HMQC and 2D NOESY data (not shown) allowed the relative orientation of the β-sheet strands to be determined. This is shown in Figure 7, which also indicates the observed interstrand NOE's. The orientation of the β-sheet strands determined in solution is identical to that seen in the crystalline state. The boundaries of the β-sheet strands match well with those of the X-ray crystal structure, with minor differences localized to the periphery. As presented here, the ends of each strand were defined by the observation of interstrand NOE's and slowly exchanging $^1H^N$ resonances. By this definition, strands B and H have one less residue and strands A and D have one additional residue on the C-terminal end than is defined by the X-ray crystal structure. As shown in Figure 7, the two carboxy-terminal stretches form parts of an interrupted strand that is connected by a type I or I′ turn to the core of the β-sheet.

Several isolated residues with slowly exchanging $^1H^N$ resonances correlate with locations of turn conformations predicted from both the X-ray crystal structure and d_{NN} NOE's. Hydrogen bonding between the carbonyl oxygen of the first residue in the turn to the backbone amide proton of the fourth residue retards exchange of the fourth-residue amide proton. This is observed for the M14, N64, and I175 $^1H^N$'s. After 1 day in ^2H_2O, the remaining $^1H^N$'s of fourth position turn residues (as defined by X-ray crystal data and d_{NN} NOE's) had exchanged away, perhaps because turns tend to be located on the surface of proteins. This is in contrast to $^1H^N$'s in the interior of the β-sheet, which we have observed to be in slow exchange on a time scale of months.

Interstrand NOE's defining the β-sheet framework, together with key NOE's, such as between W24 $^1H^{\epsilon 1}$ and I138 side-chain protons, between R65 $^1H^{\epsilon}$ and W57 $^1H^{\zeta 2}$, and between R13 $^1H^{\delta}$'s and F147 aromatic ring protons, establish that the global fold of human DHFR in solution is, as expected, qualitatively similar to that seen in the crystalline state. A quantitative solution structure determination will require more detailed side-chain assignments and a better data base of NOE constraints. We are currently using ^{13}C-labeled human DHFR

to extend our assignments to include all side-chain protons (Ikura et al., 1990a,b; Zuiderweg et al., 1990; Kay et al., 1990a,b).

Several $^1H^N$ resonances with retarded exchange rates are not involved in regular secondary structure, including two adjacent residues, G15 and I16. Reference to the X-ray crystal structure indicates that G15 can hydrogen bond to the side-chain hydroxyl of S11 and the main-chain carbonyl oxygen of N13, while I16 is positioned to form hydrogen bonds to the main-chain carbonyl oxygen of T146. Two other slowly exchanging $^1H^N$'s, those of F148 and Y156, are positioned to hydrogen bond to the main-chain carbonyl oxygens of M14 and D152, respectively.

Sequential assignment of residues in the substrate/inhibitor binding site will allow specific protein–drug and protein–substrate interactions to be determined. As an example, the F31 and L22 side chains have been found to interact with the pteridine and benzene ring systems of methotrexate. The pattern of NOE's observed from the $^1H^7$ and $^1H^{13/15}$ resonances of methotrexate to the $^1H^\epsilon$ and $^1H^\zeta$ resonances of F31 and to the $^1H^\delta$ resonances of L22 established that methotrexate binds in a nonproductive orientation (Stockman et al., 1991). In addition, only one bound conformation was observed for methotrexate. This is in contrast to what has been observed by NMR spectroscopy for *E. coli* DHFR (Falzone et al., 1991). The pattern and intensity of DHFR–ligand NOE's can be used as a basis from which to analyze changes in binding geometry that occur upon mutation of binding site residues. Analogously, binding modes of various inhibitors can be compared in this manner. The assigned $^1H^\epsilon$ of R70 will serve as a monitor of binding site changes that occur on the other side of the binding pocket, since the side chain of this residue interacts via a salt bridge with the α-carboxylate of methotrexate. The assignments of resonances in the binding pocket of the enzyme were a major goal of this research since they will allow us to characterize the conformation and mobility of various ligands, including novel antitumor drugs. Inspection of the structures of the complexes may provide hints for optimizing ligand binding and for understanding interaction specificity. Structural analysis in solution is important since the crystal structure analysis of human DHFR–ligand complexes lacks details, with respect to the conformation of bound ligands, because of unmodeled electron density in the folate-binding site (Davies et al., 1990).

A by-product of the ^{15}N-directed sequential assignment approach is the concomitant assignment of ^{15}N resonances. This will enable analysis of backbone dynamics properties of human DHFR (Clore et al., 1990). Changes in dynamic properties that occur upon binding ligand can now be addressed. This is important since the apoenzyme is quite unstable while the binary enzyme–ligand complex is stable in solution. Understanding ligand-induced dynamic changes is critical to understanding ligand-binding specificity. The ^{13}C-directed strategy of side-chain assignments will permit dynamics properties of side-chain atoms to be investigated in an analogous manner.

ACKNOWLEDGMENTS

We thank Dr. V. Thanabal and Mr. Robert Clubb for many useful discussions. We also thank Dr. Marc Adler for supplying the baseline correction routine prior to publication. We are grateful to Dr. Dennis Hare for providing the data processing software package FELIX.

REFERENCES

Adler, M. A., & Wagner, G. (1991) *J. Magn. Reson. 91*, 450–454.

Anil Kumar, Ernst, R. R., & Wüthrich, K. (1980) *Biochem. Biophys. Res. Commun. 95*, 1–6.

Bax, A., & Davis, D. G. (1985) *J. Magn. Reson. 65*, 355–360.

Bax, A., Ikura, M., Kay, L. E., Torchia, D. A., & Tschudin, R. (1990) *J. Magn. Reson. 86*, 304–318.

Birdsall, B., Feeney, J., Tendler, S. J. B., Hammond, S. J., & Roberts, G. C. K. (1989) *Biochemistry 28*, 2297–2305.

Blakley, R. L. (1984) in *Folates and Pterins* (Blakley, R. L., & Benkovic, S. J., Eds.) Vol. 1, pp 191–253, John Wiley & Sons, New York.

Bodenhausen, G., & Ruben, D. L. (1980) *Chem. Phys. Lett. 69*, 185–188.

Bolin, J. T., Filman, D. J., Matthews, D. A., Hamlin, R. C., & Kraut, J. (1982) *J. Biol. Chem. 257*, 13650–13662.

Brown, S. C., Weber, P. L., & Mueller, L. (1988) *J. Magn. Reson. 77*, 166–169.

Bystroff, C., & Kraut, J. (1991) *Biochemistry 30*, 2227–2239.

Bystroff, C., Oatley, S. J., & Kraut, J. (1990) *Biochemistry 29*, 3263–3277.

Carr, M. D., Birdsall, B., Frenkiel, T. A., Bauer, C. J., Jimenez-Barbero, J., Polshakov, V. I., McCormick, J. E., Roberts, G. C. K., & Feeney, J. (1991) *Biochemistry 30*, 6330–6341.

Clore, G. M., Driscoll, P. C., Wingfield, P. T., & Gronenborn, A. M. (1990) *Biochemistry 29*, 7387–7401.

Clubb, R. T., Thanabal, V., Osborne, C., & Wagner, G. (1991) *Biochemistry 30*, 7718–7730.

Davies, J. F., Delcamp, T. J., Prendergast, N. J., Ashford, V. A., Freisheim, J. H., & Kraut, J. (1990) *Biochemistry 29*, 9467–9479.

Edman, J. C., Edman, U., Cao, M., Lundgren, B., Kovacs, J., & Santi, D. (1989) *Proc. Natl. Acad. Sci. U.S.A. 86*, 8625–8629.

Falzone, C. J., Benkovic, S. J., & Wright, P. E. (1990) *Biochemistry 29*, 9667–9677.

Falzone, C. J., Wright, P. E. & Benkovic, S. J. (1991) *Biochemistry 30*, 2184–2191.

Fesik, S. W., Eaton, H. L., Olejinczak, E. T., Zuiderweg, E. R. P., McIntosh, L. P., & Dahlquist, F. W. (1990) *J. Am. Chem. Soc. 112*, 886–888.

Freisheim, J. H., & Matthews, D. A. (1984) in *Folate Antagonists as Therapeutic Agents* (Sirontak, F. M., Burchall, J. J., Ensminger, W. D., & Montegomery, J. A., Eds.) Vol. 1, pp 69–131, Academic Press, Orlando, FL.

Ikura, M., Kay, L. E., & Bax, A. (1990a) *Biochemistry 29*, 4659–4667.

Ikura, M., Kay, L. E., Tschudin, R., & Bax, A. (1990b) *J. Magn. Reson. 86*, 204–209.

Kay, L. E., Ikura, M., & Bax, A. (1990a) *J. Am. Chem. Soc. 112*, 888–889.

Kay, L. E., Ikura, M., & Bax, A. (1990b) *J. Magn. Reson. 91*, 84–92.

Levitt, M. H., & Freeman, R. (1981) *J. Magn. Reson. 43*, 65–80.

Marion, D., Driscoll, P. C., Kay, L. E., Wingfield, P. T., Bax, A., Gronenborn, A. M., & Clore, G. M. (1989) *Biochemistry 28*, 6150–6156.

Matthews, D. A., Bolin, J. T., Burridge, J. M., Filman, D. J., Volz, K. W., Kaufman, B. T., Beddell, C., Champness, J. N., Stammers, D. K., & Kraut, J. (1985a) *J. Biol. Chem. 260*, 381–391.

Matthews, D. A., Bolin, J. T., Burridge, J. M., Filman, D. J., Volz, K. W., & Kraut, J. (1985b) *J. Biol. Chem. 260*, 392–399.

McIntosh, L. P., & Dahlquist, F. W. (1990) *Q. Rev. Biophys. 23*, 1–38.
Morris, G. A., & Freeman, R. (1979) *J. Am. Chem. Soc. 101*, 760–762.
Oefner, C., D'Arcy, A., & Winkler, F. K. (1988) *Eur. J. Biochem. 174*, 377–385.
Piantini, U., Sørensen, O. W., & Ernst, R. R. (1982) *J. Am. Chem. Soc. 104*, 6800–6801.
Prendergast, N. J., Delcamp, T. J., Smith, P. L., & Freisheim, J. H. (1988) *Biochemistry 27*, 3663–3671.
Reddy, A. V., Behnke, W. D., & Freisheim, J. H. (1978) *Biochim. Biophys. Acta 533*, 415–427.
Shaka, A. J., Barker, P. B., & Freeman, R. (1985) *J. Magn. Reson. 64*, 547–552.
Stammers, D. K., Champness, J. N., Beddell, C. R., Dann, J. G., Eliopoulos, E., Geddes, A. J., Ogg, D., & North, A. C. T. (1987) *FEBS Lett. 218*, 178–184.
Stockman, B. J., Nirmala, N. R., Wagner, G., Delcamp, T. J., DeYarman, M. T., & Freisheim, J. H. (1991) *FEBS Lett. 283*, 267–269.
Wagner, G. (1990) *Prog. Nucl. Magn. Reson. Spectrosc. 22*, 101–139.
Wagner, G., Hyberts, S. G., & Havel, T. F. (1991) *Annu. Rev. Biophys. Biomol. Struct.* (in press).
Wüthrich, K. (1986) *NMR of Proteins and Nucleic Acids*, Wiley, New York.
Zuiderweg, E. R. P., & Fesik, S. W. (1989) *Biochemistry 28*, 2387–2391.
Zuiderweg, E. R. P., McIntosh, L. P., Dahlquist, F. W., & Fesik, S. W. (1990) *J. Magn. Reson. 86*, 210–216.

^1H and ^{15}N NMR Characterization of Free and Bound States of an Amphiphilic Peptide Interacting with Calmodulin†

Bénédicte Prêcheur,‡ Hélène Munier,§ Joël Mispelter,‖ Octavian Bârzu,§ and Constantin T. Craescu*,‡

Institut National de la Santé et de la Recherche Médicale U91 and Centre National de la Recherche Scientifique URA 607, Hôpital Henri Mondor, 94010 Créteil, France, Unité de Biochimie des Régulations Cellulaires, URA 1129, Institut Pasteur, Paris, France, and Institut National de la Santé et de la Recherche Médicale U219, Institut Curie, Orsay, France

Received July 24, 1991; Revised Manuscript Received September 26, 1991

ABSTRACT: A peptide of 17 amino acid residues Ac-L-K-W-K-K-L-L-K-L-L-K-K-L-L-K-L-G-NH_2, designed to form an amphiphilic basic α-helix [DeGrado, W. F., Prendergast, F. G., Wolfe, H. R., Jr., & Cox, J. A. (1985) *J. Cell. Biochem. 29*, 83–93], was labeled with ^{15}N at positions 1, 7, 9, and 10. Homo- and heteronuclear NMR techniques were used to characterize the conformational changes of the peptide when it binds to calmodulin in the presence of Ca^{2+} ions. The spectrum of the free peptide in aqueous solution at pH 6.3 and 298 K was completely assigned by a combined application of several two-dimensional proton NMR methods. Analysis of the short- and medium-range NOE connectivities and of the secondary chemical shifts indicated that the peptide populates, to a significant extent, an α-helix conformational state, in agreement with circular dichroism measurements under similar physicochemical conditions. ^{15}N-edited 1D spectra and $^{15}N(\omega_2)$-half-filtered two-dimensional NMR experiments on the peptide in a 1:1 complex with calmodulin allowed assignment of half of the amide proton resonances and three $C_\alpha H$ resonances of the bound peptide. The observed NOE connectivities between the peptide backbone protons are indicative of a stable helical secondary structure spanning at least the fragment L1–K11. The equilibrium and dynamic NMR parameters of the bound peptide are discussed in terms of a molecular interaction model.

Calmodulin (CaM)[1] is one of the major Ca^{2+}-dependent regulators of intracellular metabolism in eukaryotes. In the presence of Ca^{2+} ions, CaM undergoes conformational changes and can modulate the activities of a wide variety of enzymes such as protein kinases, cyclases, NAD kinases, phosphodiesterases, and calcium pumps (Cohen & Klee, 1988). Limited proteolysis and site-directed mutagenesis allowed identification of the CaM-binding sequences in several target enzymes. Despite little similarity between different CaM-binding sequences, all have in common a high proportion of basic and hydrophobic side chains, an almost complete lack of acidic side chains and a periodicity (with a three to four residue period) of hydrophobic residues along the sequence which suggests a propensity for amphiphilic α-helix secondary structure (Cox et al., 1985).

Synthetic peptides of 12–33 amino acid residues, modeled on the CaM-binding sites of various enzymes, have been shown to bind CaM in a Ca^{2+}-dependent manner. The dissociation constant of these peptides was close, if not identical to, that measured for the intact proteins, suggesting that the molecular features of the CaM/target enzyme interaction are basically reproduced in the model system. A variety of physicochemical techniques, including isotope labeling (DeGrado et al., 1985), fluorescence (Cox et al., 1985; DeGrado et al., 1985), CD (Cox et al., 1985; O'Neil et al., 1987; Garone & Steiner, 1990), X-ray and neutron diffraction (Trewhella et al., 1990), and NMR (Seeholzer et al., 1986; Klevit et al., 1985), were used

† This work was supported by grants from Centre National de la Recherche Scientifique (URA 607 and URA 1129).
* To whom correspondence should be addressed.
‡ Hôpital Henri Mondor.
§ Institut Pasteur.
‖ Institut Curie.

[1] Abbreviations: CaM, calmodulin; CD, circular dichroism; NMR, nuclear magnetic resonance; 2D, two dimensional; COSY, *J*-correlated spectroscopy; RCOSY, relayed correlated spectroscopy; TOCSY, total correlation spectroscopy; NOESY, nuclear Overhauser enhancement spectroscopy.

0006-2960/92/0431-229$03.00/0